Radiation resistance of FC.92

Myeongkyu Lee, Geon Kim, Jungsu Ahn, Sangjoon Ahn*
Department of Nuclear Engineering, Ulsan National Institute of Science and Technology (UNIST)
50 UNIST-gil, Ulsan, Republic of Korea, 44919
**Corresponding author:sjahn99@unist.ac.kr*

1. Introduction

FC.92 is a newly developed ferritic/martensitic (F/M) steel to be used in Prototype Gen-IV Sodium-cooled Fast Reactor (PGSFR) as a cladding material. Superior mechanical properties of the steel compared to other advanced F/M steels, especially high temperature creep strength, have been reported from a few prior studies [1] and now its overall radiation performance test is ongoing in BOR-60(Russia).

While the in-pile irradiation test is producing limited range data, only effective for the particular set of reactor operating parameters, we conducted a series of ion beam irradiation tests to separately assess the radiation resistance of the FC.92. To achieve the comparative study, four F/M steels (HT.9, Gr.92, FC.92-B, and FC.92-N) were selected purposely and irradiated up to ~200 dpa using 60-keV helium ion beam accelerator.

2. Experimental

2.1. Specimen preparation and ion-beam irradiation

As-received alloy plates of the four F/M steels were sectioned into cuboids (10 mm × 10 mm × 4 mm) by electrical discharge machining. The sectioned specimen surface (to be irradiated) was flattened using SiC papers and polished with 0.25 μm diamond suspension. The prepared specimens were irradiated with 60 keV helium ion (fluence: 2.47×10^{18} ions/cm^2) using Korea Multi-purpose Accelerator Complex (KOMAC) accelerator.

2.2. Characterization of irradiated specimen

Irradiated specimens (7 μm × 5 μm × 100 nm) were prepared using focused ion beam (FIB, FEI Helios 450HP) with lift-out technique. Bright-field (BF) and high angle annular dark-field (HAADF) images were collected using a high-resolution transmission electron microscope (HR-TEM, JEOL JEM-2100). Comparative image analysis on irradiation-induced voids and gas bubbles formed in the steels was conducted using ImageJ(FIJI) mainly in the standpoint of penetration depth and swelling.

2.3. Conventional SRIM simulation

Figure 1 shows typical conventional SRIM simulation results obtained from FC.92-B adopting

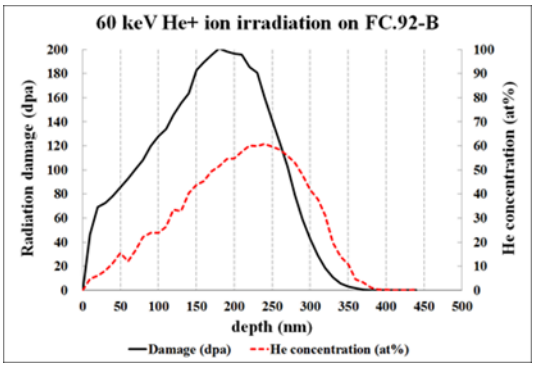

Figure 1. Radiation damage and He distribution in FC.92-B irradiated with 60 keV He^+ ion-beam at the fluence of 2.47×10^{18} ions/cm^2 (SRIM-2013)

'Detailed Calculation with Full Damage Cascades' option and 40 eV displacement threshold energy referring to the ASTM standard [2]. For all tested steels, conventional SRIM simulation predicted very similar results, which is not at all surprising considering the calculation logic behind the program, however completely not matching with experimental results of this study based on excessively high dose helium irradiation.

2.4. Multi-step SRIM simulation for high dose ion irradiation

To properly reflect effective target density reduction and helium concentration increase during irradiation, multi-step SRIM simulations were carried out by updating target density and alloy compositions for optimized time steps and layer thicknesses determined from the sensitivity study.

3. Results and discussion

3.1. Quantitative analysis of helium bubble formation

Figures 2 and 3 highlight the remarkably different radiation responses of the tested F/M steels. Foremost difference is the helium ion penetration depth summarized in Table 1, which vary from 590 nm to 1400 nm, unlike the conventional SRIM simulation results shown in Fig. 1. Alloy FC.92-B exhibited much shallow penetration depth compared to other

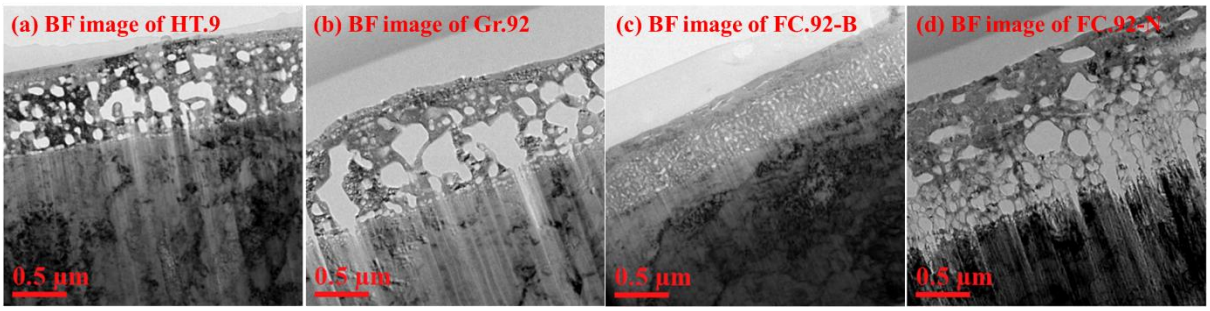

Figure 2. Bright field(BF) images of FMS specimens irradiated by 60-keV helium ions with a radiation damage of 200 dpa

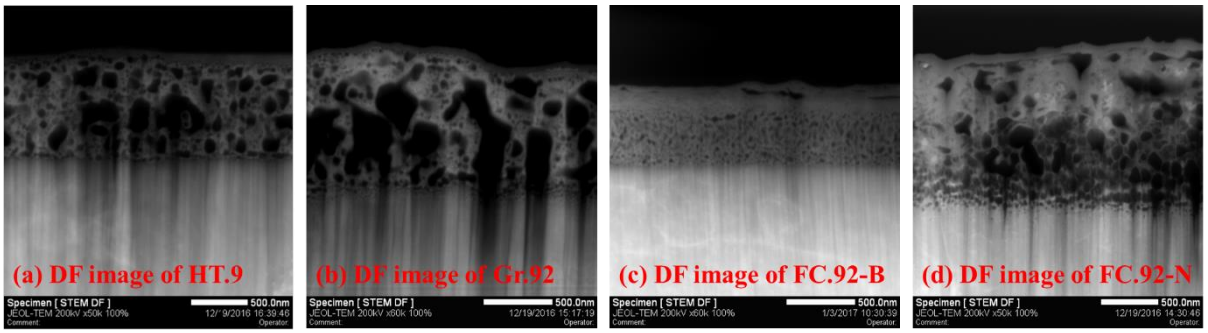

Figure 3. Dark field(DF) images of FMS specimens irradiated by 60-keV helium ions with a radiation damage of 200 dpa

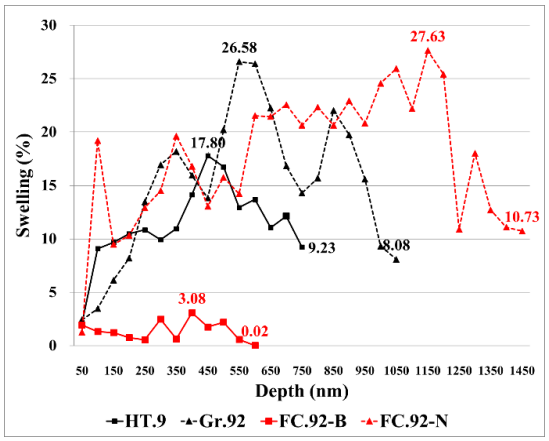

Figure 4. Swelling of irradiated FMS specimens over irradiated regions

three alloys. However, in all irradiated alloys, radiation damaged structure was observed beyond SRIM-predicted penetration limit (~380 nm) with broadened radiation damage peak. This broadening of radiation damage peak is likely due to *in-situ* decrease of atomic density or macroscopic stopping power of the alloy target.

Outstanding alpha-ray resistance of FC.92-B among the tested can be reaffirmed from the swelling versus depth profile shown in Fig. 4. Regional swelling values were obtained from average radius and number density in every 50-nm sectioned TEM image using the equation,

$$\text{Swelling } S = \Delta V / V = \Sigma \frac{4}{3}\pi r_{\text{average}}^3 / V , \quad (1)$$

where r_{average} and V present average radius of voids and bubbles, and the actual volume of irradiated regions imaginarily-sectioned on the TEM images. In contrast to numerous number of large (> 20 nm) long-torn bubbles found from HT.9, Gr.92, and FC.92-N, bubble growth in FC.92-B were relatively limited to small spherical bubbles. The maximum swelling near radiation damage peak (estimated to be located at ~150 nm) of FC.92-B was only 3.1%, as compared to 17.8% in HT.9, 26.6% in Gr.92, and 27.6% in FC.92-N, respectively.

	Penetration depth (nm)	Maximum swelling (%)	Minimum swelling (%)
HT.9	771.7	17.79	2.41
Gr.92	1048.8	26.58	2.42
FC.92-B	591.9	3.08	0.02
FC.92-N	1400.5	27.63	1.27

Table 1. Quantitative analysis of microstructural deformation in irradiated F/M steels

3.2. Comparison between conventional and multi-step SRIM simulation

To establish the multi-step simulation procedure, FC.92-B was selected for a reference steel since least amount of interconnected bubbles were found and various parameters listed in Table 2 were tested for the sensitivity study to determine optimized imaginary layer thickness and irradiation time step. Figures 5 and 6 show the effects of each parameter on simulation

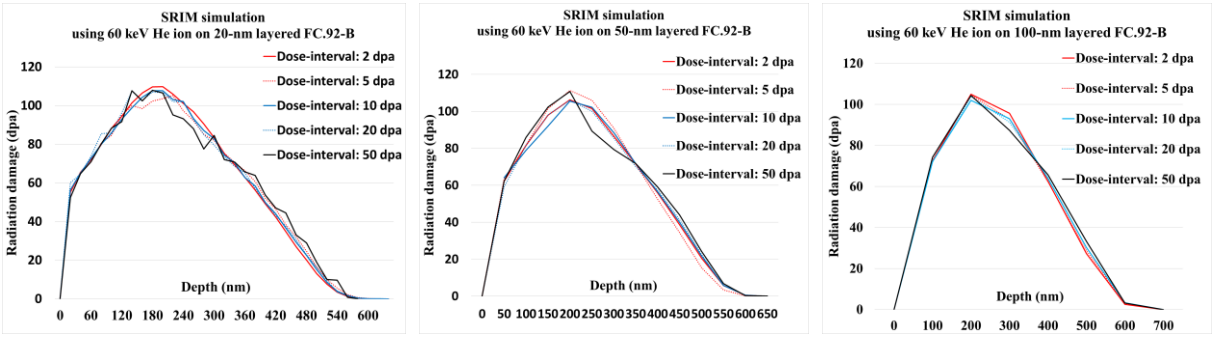

Figure 5. Multi-step SRIM simulation results with fixed layer thickness

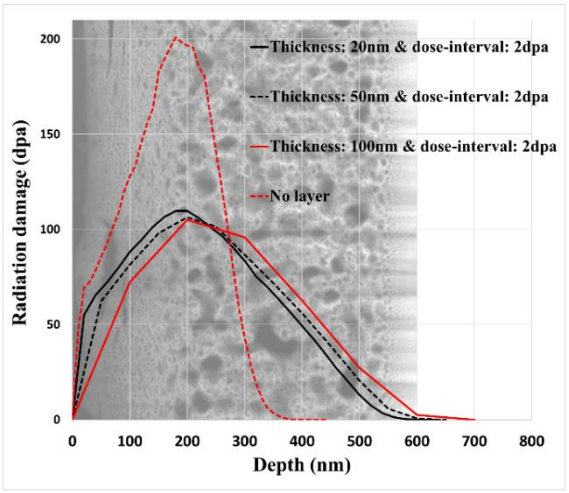

Figure 6. Radiation damage profiles from conventional and multi-step SRIM simulations

results, which suggest 10 dpa dose-step and 100 nm layer thickness are both reasonably small enough to yield more acceptable predictions matching with the experimental results.

Although multi-step simulation with the optimized parameters yielded more matching penetration depth with broadened radiation damage peak as shown in Fig. 6, however porosity distribution trend is not perfectly following the simulation results. This could be due to vacancy assumption for implanted helium atoms based on the low solubility and high mobility of helium atoms in stainless steels.

In terms of penetration depth, multi-step SRIM simulation predicted much more accurate results than its conventional counterpart, matching with experimental data within 5% error, especially in case of FC.92-B. It should be noted that achieved maximum dpa in the target is only ~110 dpa in multi-step calculation, since the radiation damage is distributed over at least twice wider range than that of conventional simulation for the steel. However, further modification of multi-step SRIM simulation is required to reflect metallurgical characteristics of the other three steels that exhibited up to twice wider penetration depth than that of FC.92-B.

4. Conclusion

Alloy FC.92-B exhibited at least 25% reduced helium ion penetration (~590 nm) and 20% less swelling (~3.1% at damage peak) compared to HT.9, Gr.92, and FC.92-B, under excessive irradiation of 60-keV helium ions (fluence: 2.47×10^{18} ions/cm^2). Radiation damage peak broadening and unexpectedly deep penetration depth than conventional SRIM simulation was the common observation from all tested steels. Rudimentary multi-step SRIM simulation successfully handled mismatches between theoretical predications and experimental observation for this study. However, further modification is surely required for SRIM to comprehend differential porosity development due to alloy microstructure.

5. Acknowledgements

We appreciate the KAERI and KOMAC for providing F/M steels and helium irradiation time. This research was supported by the National Research Foundation of Korea (NRF) grant funded by the Korean Government (MSIP: Ministry of Science, ICT and future Planning) (No. 2016M2BA9912471)

References

[1] J. Yoo, J. Chang, J.-Y. Lim, J.-S. Cheon, T.-H. Lee, S.K. Kim, K.L. Lee, H.-K. Joo, Overall System Description and Safety Characteristics of Prototype Gen IV Sodium Cooled Fast Reactor in Korea, Nuclear Engineering and Technology 48(5) (2016) 1059-1070.

[2] Standard Practice for Characterizing Neutron Exposures in Iron and Low Alloy Steels in Terms of Displacements Per Atom (DPA).